

Observed trends in light precipitation events over global land during 1961–2010

Guanhuan Wen¹ · Gang Huang^{2,3} · Weichen Tao² · Chunxia Liu¹

Received: 12 December 2014 / Accepted: 30 April 2015 / Published online: 13 May 2015
© Springer-Verlag Wien 2015

Abstract Based on daily station precipitation data, this study investigates the trends in light precipitation events (less than the 50th percentile) over global land during 1961–2010. It is found that the frequency of light precipitation events decreases over East China (EC) and northern Eurasia (NE) but increases over the United States of America (US), Australia (AU), and the Iberian Peninsula (IP). However, the trends in the intensity of light precipitation events are opposite to those in frequency. We find that the trends in light precipitation events are possibly associated with the changes in static stability. Over EC and NE (US, AU, and IP), the static stability weakens (strengthens) during 1961–2010. The weakening (strengthening) of static stability leads to increase (decrease) in precipitation intensity due to the enhancement (reduction) of upward motion; light (relatively heavier) precipitation events accordingly shift toward relatively heavier (light) precipitation, and the frequency of light precipitation events decreases (increases) consequently.

1 Introduction

Observations show that the global mean surface temperature has increased steadily since the beginning of the twentieth

century and this warming trend is particularly strong over the past few decades (Trenberth et al. 2007). Global warming is supposed to have a noticeable impact on global and regional hydrological cycle (Trenberth 1999, 2011; Held and Soden 2006). The warming climate results in an increase in evaporation and atmospheric moisture content, which in turn leads to enhancement of total precipitation and heavy precipitation (Trenberth 1999; Karl and Trenberth 2003; Trenberth et al. 2003; Allan and Soden 2008).

Additionally, it is expected that heavy precipitation increases more than total precipitation based on theory and numerical models (Hennessy et al. 1997; Allen and Ingram 2002; Trenberth et al. 2003; Pall et al. 2007; Liu et al. 2009; Shiu et al. 2012). Trenberth et al. (2003) hypothesized that heavy precipitation should increase at about the same rate as atmospheric moisture that increases 7 % per Kelvin according to the Clausius–Clapeyron relation. What is more, they argued that the increase in heavy precipitation could even exceed 7 % per Kelvin because of additional latent heat released from the increasing water vapor. Climate models also support this result despite different increasing magnitudes. On the other hand, global mean precipitation increases at the same rate as global evaporation which is constrained by global energy budget (Boer 1993; Trenberth 1998). It is found that the increasing rate of total precipitation is about 1–3 % per Kelvin (Allen and Ingram 2002; Held and Soden 2006; Sun et al. 2007). Thus, the increase in heavy precipitation is more than that in total precipitation. The implication is that there must be a decrease in relatively weaker precipitation events (Trenberth et al. 2003).

Observed records indicate that there are widespread increases in heavy precipitation events over global land in recent warming decades (Groisman et al. 1999, 2005; Easterling et al. 2000; Alexander et al. 2006). Significant increases in the heavy precipitation events have been reported over lots of land areas, such as the USA (Karl and Knight 1998; Kunkel et al. 1999), Canada (Zhang et al. 2001), the UK (Osborn et al.

✉ Gang Huang
hg@mail.iap.ac.cn

¹ Guangzhou Institute of Tropical and Marine Meteorology/
Guangdong Provincial Key Laboratory of Regional Numerical
Weather Prediction, China Meteorological Administration,
Guangzhou 510080, China

² State Key Laboratory of Numerical Modeling for Atmospheric
Sciences and Geophysical Fluid Dynamics, Institute of Atmospheric
Physics, Chinese Academy of Sciences, Beijing 100029, China

³ Joint Center for Global Change Studies, Beijing 100875, China

2000), Europe (Klein Tank and Können 2003), Northern Eurasia (Wen et al. 2015), Japan (Fujibe et al. 2005), Northwest and South China (Zhai et al. 2005), India (Goswami et al. 2006), and Australia (Suppiah and Hennessy 1998). Thus, the observations support the expectation that there would be increases of heavy precipitation in warming climate.

Theory and climate models indicate that heavy precipitation increases at the cost of light precipitation. The light precipitation would decline while the heavy precipitation rises. Increases of heavy precipitation events are widespread over global land areas. So it is reasonable to ask whether the light precipitation events over land have decreased globally. To answer this question, we collect a large number of observed daily precipitation data covering a large part of global land and use uniform method to define light precipitation event. We analyze the trends in light precipitation events based on observed data. Moreover, we discuss possible reason for the trends in light precipitation events using reanalysis data and numerical model as well.

The rest of this paper is organized as follows: section 2 introduces data, methods, and model; and section 3 describes the trends in light precipitation events over global land. A possible reason for the trends in light precipitation events is discussed in section 4. Finally, conclusions and discussions are given in section 5.

2 Data, methods, and model

2.1 Data

Daily station precipitation data from several organizations are used in this study. These include Global Historical Climatology Network (GHCN) daily precipitation dataset (Menne et al. 2012) from the National Climate Data Center (NCDC), European station daily precipitation dataset (Klein Tank et al. 2002) from European Climate Assessment and Dataset (ECA&D) project, and Chinese station daily precipitation dataset from China Meteorological Administration (CMA). The GHCN dataset contains more than 70,000 stations across global land except the Antarctic (Menne et al. 2012). The lengths of the records span from more than one century to several years. However, most of the data in South America and Africa is not long enough to detect climate change. What is more, the quality of GHCN data over Europe and China is poorer than that in the data from ECA&D project and CMA, which contain more stations and less missing records. Thus, we replace the precipitation data over Europe and China in GHCN dataset with those from ECA&D project and CMA.

Date quality control is taken into account in order to ensure the reliability of the results in this study. NCDC has applied a set of quality assurance procedures to GHCN dataset to detect duplicate data, climatological outliers, and various

inconsistencies (Durre et al. 2010). ECA&D project has also checked the European station daily precipitation dataset and detected data errors such as climatological outliers and negative values. The daily precipitation dataset from CMA is also quality controlled by detecting the climatological outliers, negative values, and world record exceedances, referring to the quality checks applied to GHCN dataset (Durre et al. 2010). The records failing in quality checks are regarded as missing values, and the records passing all the checks are taken as reliable values.

We select stations with data long enough based on some standards after quality control. A year with no missing value is classified as a usable year. A station with 40 or more usable years during 1961–2010 is accepted. As a result, 3538 stations across global land, shown in Fig. 1a, are picked up. However, there are few stations over South America and Africa. Thus, the trends in light precipitation events in these two continents are not analyzed in this study.

Atmospheric data used, including monthly mean temperature, geopotential height, and precipitable water, are derived from the National Centers for Environmental Prediction and National Center for Atmospheric Research (NCEP-NCAR) atmospheric reanalysis dataset (Kalnay et al. 1996). The data have a $2.5 \times 2.5^\circ$ horizontal resolution and extend from 1000 to 10 hPa with 17 pressure levels in vertical. The data is available from January 1948.

2.2 Methods

Precipitation event with daily precipitation less than 10 mm/day is commonly regarded as light precipitation event (Qian et al. 2009, 2010). According to this definition, light precipitation events account for a large part of the total over land, about 50–80 % at mid latitudes and more than 90 % at high latitudes and other arid and semi-arid areas (Huang and Wen 2013). Thus, a fixed threshold to define light precipitation event may be inappropriate. We want the light precipitation event defined in this study to represent the bottom tail of daily precipitation probability distribution. Furthermore, there are significant regional differences in precipitation. Therefore, we use percentile threshold to define light precipitation event. The 50th percentile based on 30-year (1971–2000) daily precipitation data is chosen to be the threshold for light precipitation event. The 50th percentile is defined as the middle value among daily precipitation of 0.1 mm/day or more. A day with daily precipitation greater than or equal to 0.1 mm/day is regarded as a precipitation day. For each station, if daily precipitation is less than the corresponding threshold (the 50th percentile) and greater than or equal to 0.1 mm/day, then the precipitation event on that day is taken as a light precipitation event. The threshold for each station was calculated. Annual and seasonal thresholds, shown in Fig. 1b–d, are computed separately. The thresholds for most regions are around 1–

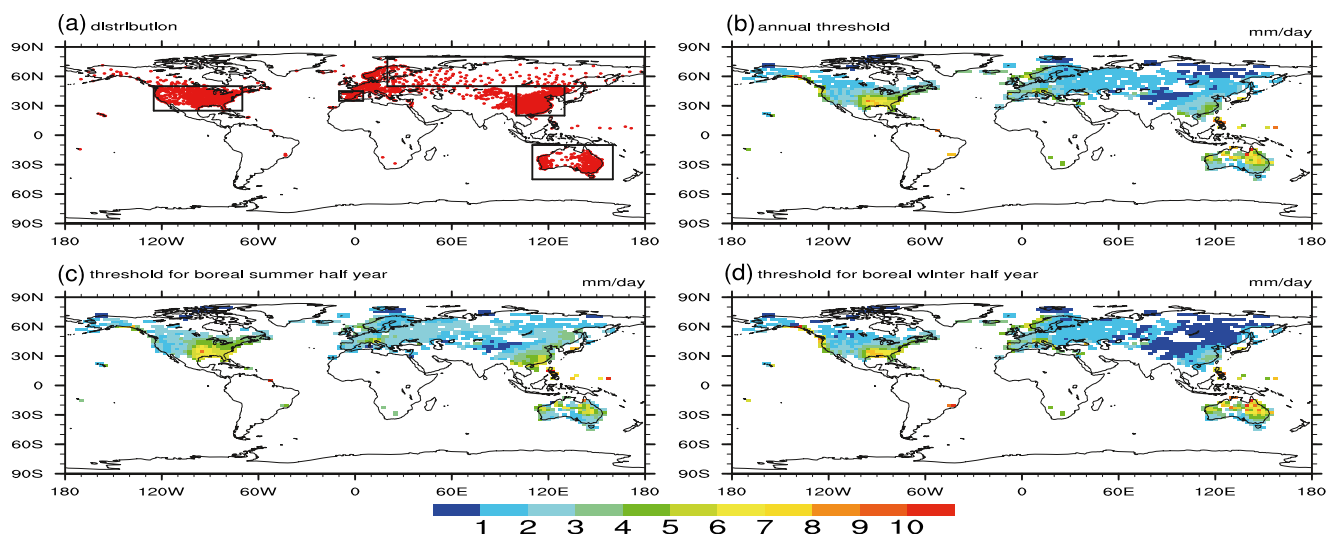


Fig. 1 a Locations of 3538 precipitation stations (red dots) used and the five regions (black rectangles) analyzed in this study and threshold values (mm/day) for b the whole year, c boreal summer half year, and d boreal

winter half year. The scale bar at the bottom of figure is used for measuring the threshold values and the unit is mm/day

5 mm/day. In general, the threshold at lower latitudes and wet regions are larger than those at higher latitudes and arid regions. The thresholds for boreal summer half year are generally larger than annual thresholds, and those for boreal winter half year are less than annual thresholds. In addition, we want to point out that similar results are obtained when either 30th or 40th percentile is used as the threshold to define light precipitation event.

Considering the seasonal differences of climate background, this study divides a year into boreal summer half year and boreal winter half year and analyzes the trends of light precipitation events in boreal summer and winter half years, respectively. Same as the study of Zhai et al. (2005), boreal summer half year is from April to September and boreal winter half year is from October to March in the next year. Linear regression is used to analyze long-term trends and Student's *t* test is used to examine the significance of the trends.

The stations available for this study are not evenly distributed across the global land areas. Thus, a gridding method is needed to interpolate the results onto regular latitude-longitude grid. New et al. (2000) find that angular distance weighting (ADW) algorithm (Shepard 1968, 1984) is the most appropriate method for gridding irregularly spaced data when comparing to several other methods. Several studies have used a modified ADW algorithm to grid daily climate extreme indices (Kiktev et al. 2003), such as maximum and minimum temperature (Caesar et al. 2006) and heavy precipitation events (Alexander et al. 2006). The global gridded climate extremes indices, HadEX and HadEX2, managed by the Met Office Hadley Centre, are based on this method. A more detail description about this method is documented by Alexander et al. (2006). The gridding method in this study is the same as that used by Alexander et al. (2006) except for differences

in some parameters. The minimum number of stations required to calculate a grid point value is one, which is less than previous works (Alexander et al. 2006; Donat et al. 2013). The search radius is fixed to 200 km, which is close to the length of the grid used. We calculate the anomaly and climate mean (averaged during 1971–2000) of the indices relative to light precipitation events separately for each station and then interpolate them onto $2.5 \times 2.5^\circ$ latitude–longitude grid using ADW method.

2.3 Model and experimental design

This study utilizes the Advanced Research Weather Research Forecasting (ARW-WRF) model (version 3.4.1) developed by NCAR, NCEP, and others. We use a 30-km horizontal grid resolution and 28 terrain-following vertical layers. The model domain is centered at 55°N and 30°E and consists of 201 (west–east) \times 111 (south–north) grid points. The model's initial conditions and outmost lateral boundary conditions are obtained from the National Centers for Environmental Prediction (NCEP) global final (FNL) analysis dataset (National Centers for Environmental Prediction 2000) at $1 \times 1^\circ$ horizontal resolution and 6-h intervals.

The following three experiments are performed using the above model: control experiment CTL and sensitivity experiments WEA and STR. In the CTL run, the initial condition and lateral boundary condition for the model are derived from NCEP-FNL analysis data. The initial condition and lateral boundary condition for STR and WEA are the same as those for CTL except for temperature field. In the WEA runs, the temperatures from 1000 to 200 hPa in the initial conditions and lateral boundary conditions are added by 1.8–0.0 K at an interval of 0.1 K, in order to increase the lapse rate and weaken

the static stability. In contrast, in the STR runs, the temperatures from 1000 to 200 hPa in the initial condition and lateral boundary condition are added 0.0–1.8 K at an interval of 0.1 K, which decreases the lapse rate and strengthens the static stability. All the three experiments are repeated for 30 times with each run integrated 24 h starting from 0000 UTC of every day in July and January 2009 except for the last day of the 2 months, respectively. A summary of all the three experiments is given in Table 1.

3 Trends in light precipitation events over global land during 1961–2010

We first analyze the trends in annual light precipitation events. Considering the seasonality, we investigate the trends in boreal summer and winter half year further.

3.1 Trends in annual light precipitation events

Frequency, intensity, and amount are the three aspects of precipitation events. The intensity is the amount divided by the frequency. Thus, we calculate the long-term trends in the frequency, intensity, and amount of light precipitation events, respectively. The result is shown in Fig. 2.

There are evident regional differences for the trends in the frequency of light precipitation events (Fig. 2). There are decreasing trends over East China (EC) and northern Eurasia (NE, refer in particular to the area north of 50°N and east of 20°E), but increasing trends over the United States of America (US), Australia (AU), and the Iberian Peninsula (IP). The frequency of light precipitation events is reduced by 3.0 % per decade (Fig. 3a) over EC (100–130°E, 20–50°N) and by 2.5 % per decade (Fig. 3d) over NE (20–180°E, 50–80°N). Both decreasing trends are significant at more than 99.9 % confidence level according Student's *t* test (Fig. 3a, d). In contrast, the frequency of light precipitation events increases by 0.8 % (Fig. 3g), 3.1 % (Fig. 3j), and 2.7 % (Fig. 3m) per decade over US (70–125°W, 25–50°N), AU (110–160°E, 10–

Table 1 Summary of model experiment design

Experiment	Initial and boundary conditions	Sample size	
		July	January
CTL	Directly from FNL data	30	30
WEA	Same as those for CTL expect temperature field. The temperatures at 1000–200 hPa are added 1.8–0.0 K at an interval of 0.1 K	30	30
STR	Same as those for CTL expect temperature field. The temperatures at 1000–200 hPa are added 0.0–1.8 K at an interval of 0.1 K	30	30

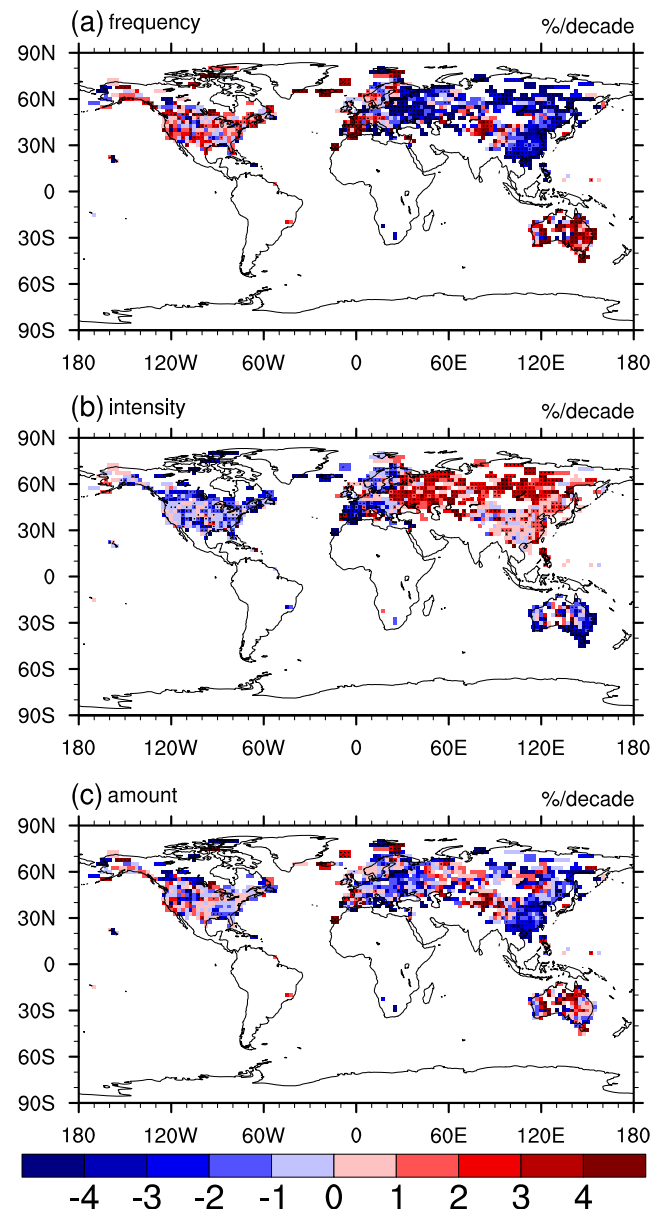


Fig. 2 Trends (%/decade, relative to climatology, which is the mean during 1971–2000; climatology period is the same hereafter) in annual **a** frequency, **b** intensity, and **c** amount of light precipitation events over land. *Black dots* denote the grid points where the trend is significant at 90 % confidence level according to Student's *t* test

45°S), and IP (10°W–5°E, 35°–45°N), respectively. The trends over AU (Fig. 3j) and IP (Fig. 3m) are both significant exceeding the 99 % confidence level, and the trend over US (Fig. 3g) is also significant above the 95 % confidence level.

The intensity of light precipitation events has changed significantly as well. The changes in intensity are characterized by increasing trends over EC and NE but decreasing trends over US, AU, and IP (Fig. 2b), which are opposite to those in frequency. The intensity of light precipitation events is increased significantly by 0.9 % (Fig. 3b) and 1.7 % (Fig. 3e) per decade over EC and NE,

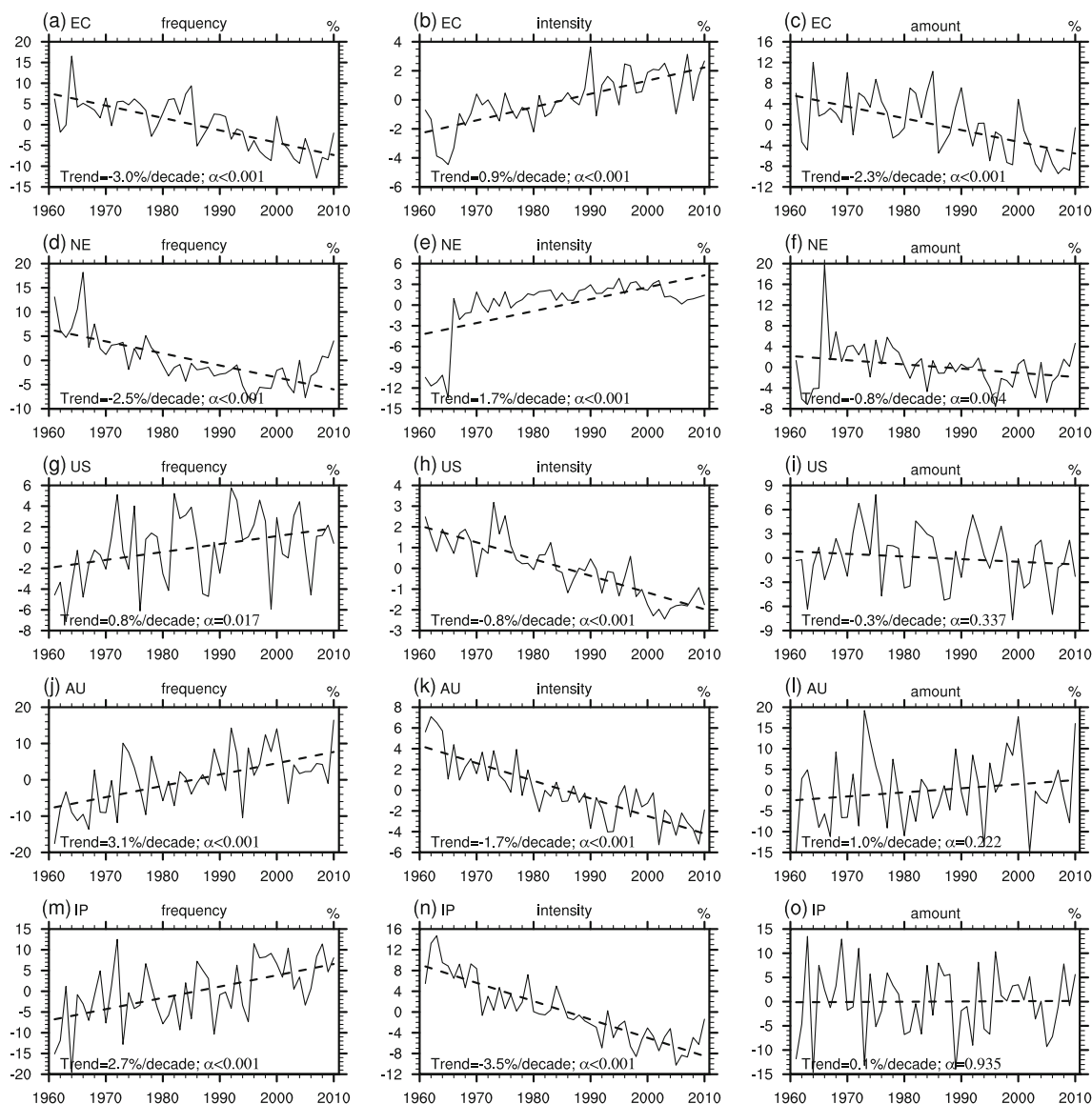


Fig. 3 Anomaly percentage (% *solid line*) of regional average frequency (*left column*), intensity (*second column*), and amount (*right column*) of light precipitation events during 1961–2010 over East China (EC, *top row*),

northern Eurasia (NE, *second row*), United States of America (US, *third row*), Australia (AU, *fourth row*), and the Iberian Peninsula (IP, *bottom row*), respectively. *Dashed lines* represent the trends (%/decade)

respectively. In contrast, the intensity of light precipitation events is decreased by 0.8 % (Fig. 3h), 1.7 % (Fig. 3k), 3.5 % (Fig. 3n) per decade over US, AU, and IP, respectively. The trends in the intensity of light precipitation events are all significant at more than 99.9 % confidence level over the five regions (Fig. 3b, e, h, k, n).

However, there are no spatially consistent trends in the amount of light precipitation events over most of land such NE, US, AU, and IP, except for EC (Fig. 2c). The regional average light precipitation amount does not have evident trend over NE (Fig. 3f), US (Fig. 3i), AU (Fig. 3l), and IP (Fig. 3o), since the linear trends are small and insignificant at the 95 % confidence level. This is due to opposite trends in the frequency and intensity.

3.2 Trends in light precipitation events in boreal summer and winter half year

We further investigate the trends in the frequency, intensity, and amount of light precipitation events in boreal summer and winter half year, which are shown in Fig. 4.

The spatial pattern of trends in frequency for boreal summer half year (Fig. 4a) resembles that for boreal winter half year (Fig. 4b). There are spatial coherent decreasing trends in the frequency of light precipitation events over EC and NE. The regional average frequency for boreal summer and winter half year is reduced by 2.9 and 2.6 % per decade over EC, and 2.4 and 2.2 % per decade over NE, respectively (Table 2). In contrast, increasing trends

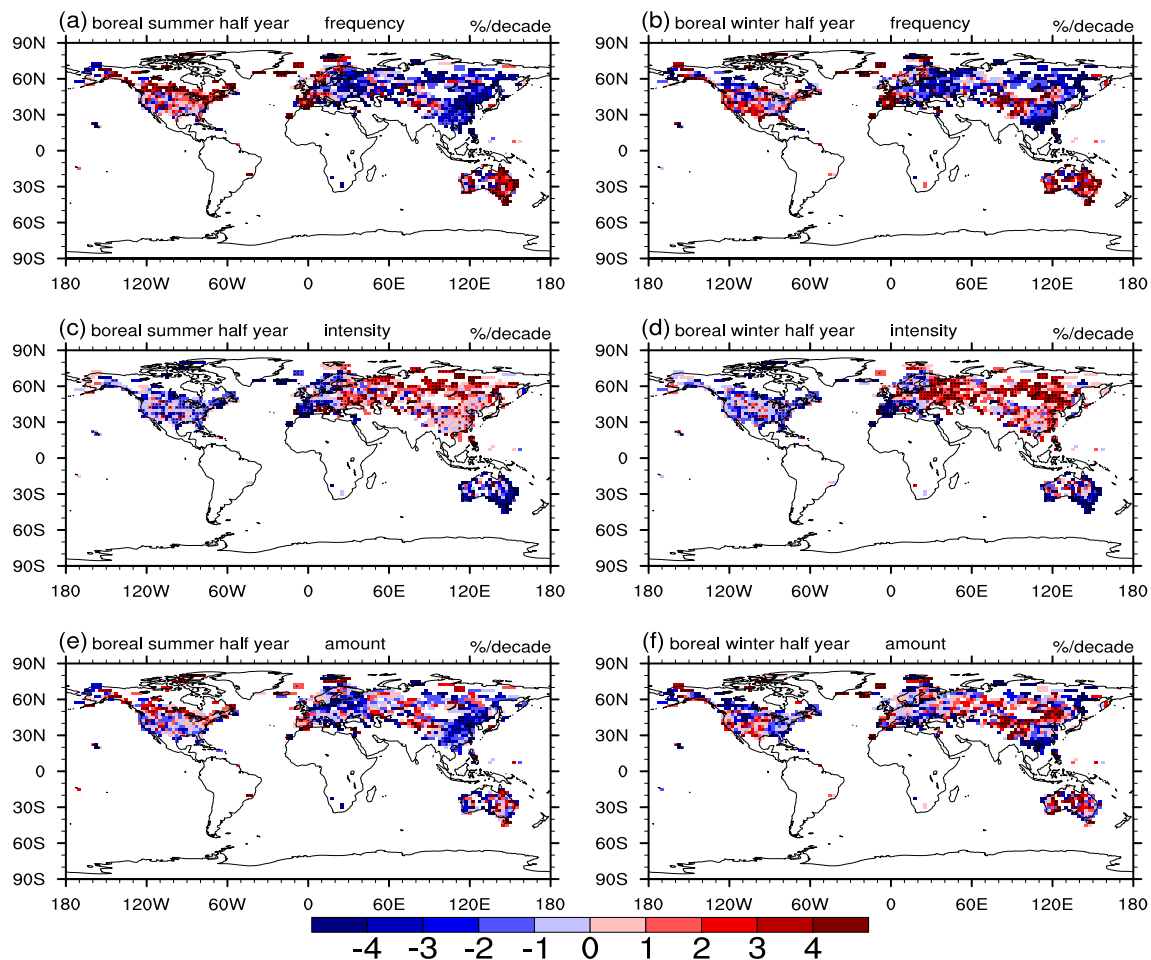


Fig. 4 Trends (%/decade) in frequency (*top row*), intensity (*second row*), and amount (*bottom row*) of light precipitation events in boreal summer (*left column*) and winter (*right column*) half year. Black dots denote the

grid points where the trend is significant at 90 % confidence level according to Student's *t* test

are widespread over US, AU, and IP in both boreal summer (Fig. 4a) and winter (Fig. 4b) half year. The frequency of light precipitation events for boreal summer half year increases by 1.0, 3.1, and 3.2 % per decade, and that for boreal winter half year increases by 0.5, 3.4, and 3.3 % per decade over US, AU, and IP, respectively (Table 2). The trends in regional average frequency are all significant at the 99 % confidence level except for that in boreal winter half year over US.

Significant trends in the intensity of light precipitation events are also found in boreal summer (Fig. 4c) and winter (Fig. 4d) half year. What is more, the spatial patterns are quite similar. However, the trends in intensity are opposite to those in frequency. There are spatially coherent enhancing trends in intensity over EC and NC but reducing trends over US, AU, and IP. The intensity for boreal summer and winter half year is increased by 0.7 and 1.5 % per decade over EC and 1.2 and 1.9 % per decade over NE, respectively (Table 2). By

Table 2 Trends (%/decade) in light precipitation events in boreal summer (Sum) and winter (Win) half year over East China (EC), northern Eurasia (NE), United States of America (US), Australia (AU), and the Iberian Peninsula (IP), respectively

	Frequency		Intensity		Amount	
	Sum	Win	Sum	Win	Sum	Win
EC	-2.9***	-2.6***	0.7***	1.5***	-2.1***	-1.9**
NE	-2.4***	-2.2***	1.2***	1.9***	-1.3***	-0.2
US	1.0***	0.5	-0.8***	-0.8***	-0.1	-0.5
AU	3.1***	3.4***	-2.3***	-1.4***	0.0	1.3
IP	3.2***	3.3***	-3.6***	-4.2***	0.6	0.3

*, **, and *** indicate the trends significant at the 90, 95, and 99 % confidence level according to Student's *t* test

comparison, the intensity for both boreal summer and winter half year is decreased by 0.8 % per decade over US (Table 2). The decreasing trends are more dramatic over AU and IP, where the intensity reduces by 2.3 and 3.6 % per decade in boreal summer half year and reduces by 1.4 and 4.2 % per decade in boreal winter half year (Table 2). All the trends in regional average intensity are significant at the 99 % confidence level (Table 2).

However, there is no distinct spatial consistence for the trend in the amount of light precipitation events in both boreal summer (Fig. 4e) and winter (Fig. 4f) half year. Magnitudes of most of the trends in regional average amounts are less than 1.0 % per decade and even insignificant at the 90 % confidence level (Table 2). This is because of the opposite trends in frequency and intensity.

In general, the trends in light precipitation events are quite similar in boreal summer and winter half years. The frequency decreases and the intensity increases over EC and NE, but there are opposite trends over US, AU, and IP.

4 Possible reason for the trends in light precipitation events

Previous studies (Trenberth et al. 2003; Trenberth 2011) suggest that the frequency of light precipitation events would

decrease following global warming. However, observed trends here indicate that there is no widespread reduction in light precipitation events over land in recent decade. Although Most of Eurasia including EC and NE exhibits a significant decreasing trend, the increase in the frequency of light precipitation events is common over US, AU, and IP. Hence, the reasons for the trend in light precipitation events should be investigated further.

4.1 Trends in precipitable water during 1961–2010

Water vapor is one of the important factors affecting precipitation. Figure 5a and b show the trend in total column precipitable water in boreal summer and winter half year during 1961–2010. The precipitable water is decreased over EC but is increased over NE in both boreal summer (Fig. 5a) and winter (Fig. 5b) half year. However, the light precipitation events exhibit the same trends over EC and NE. In addition, the precipitable water rises over US but declines over IP in boreal summer and winter half year. There are inverse trends in precipitable water between US and IP, but there are the same trends in light precipitation events. The precipitable water in boreal summer does not show spatially coherent trend over AU where the frequency of light precipitation events is mainly increased. What is more, the

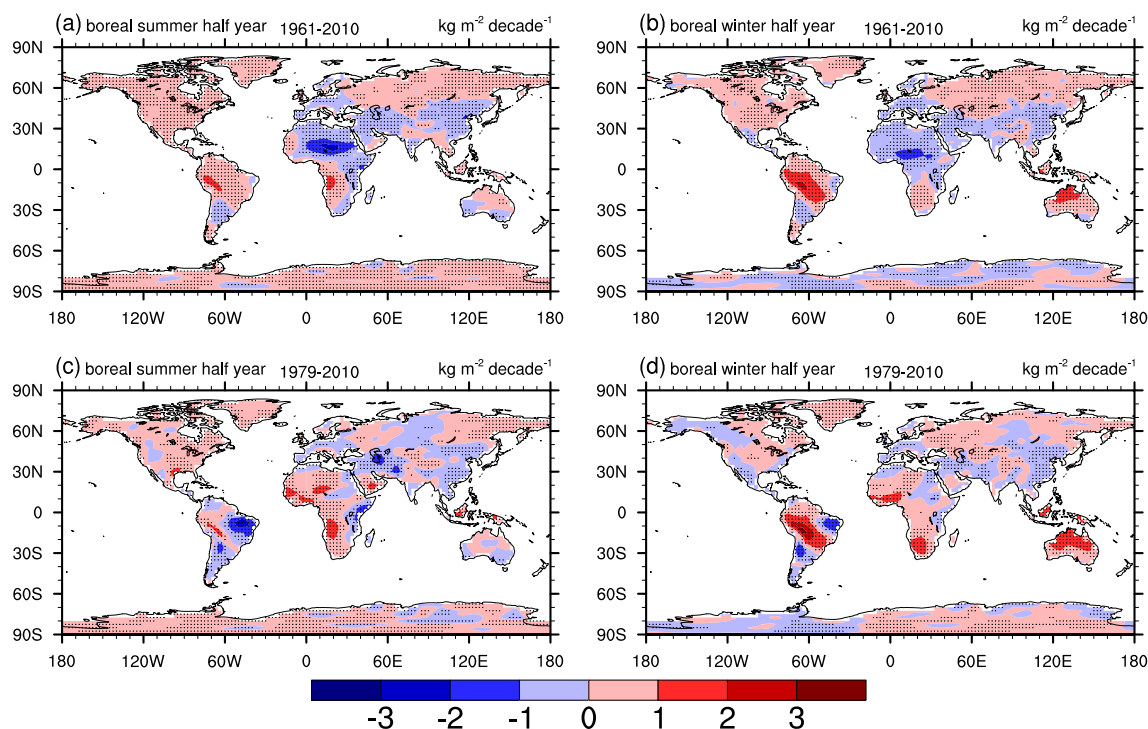


Fig. 5 Trends ($\text{kg m}^{-2} \text{decade}^{-1}$) in total column precipitable water in boreal summer (left column) and winter (right column) half year during 1961–2010 (top row) and 1979–2010 (bottom row) based on NCEP-

NCAR reanalysis data. Black dots denote the grid points where the trend is significant at 90 % confidence level according to Student's *t* test

precipitable water consistently rises over NE and US in both boreal summer and winter half year, but the trends in light precipitation events are opposite. Hence, there are no creditable linkage between the trends in light precipitation events and atmospheric water vapor.

The reliability of the trend detected by reanalysis data is often cared about for the change in observing system. The global observing system experienced three major stages: the “early” period from 1940s to the International Geophysical Year in 1957, when the first global-scale upper-air observations were established; the “modern rawinsonde network” from 1958 to 1978; and the “modern satellite” era from 1979 to the present (Kistler et al. 2001; Zverev and Chu 2003). The change in observing system makes it more difficult to detect trend associated with climate change. Even so, there are some ways to test the reliability of the reanalysis data. Computing trends for the period after 1979 and comparing with other reanalysis data or observation data are commonly suggested and used (Kistler et al. 2001). Figure 5 shows the trends in precipitable water for the investigation period of 1961–2010 and the satellite period of 1979–2010. It can be seen that the pattern of the trends are generally similar between the two periods though there are some difference in some regions. Over EC and IP, the trends for boreal summer and winter half year are both decrease during 1979–2010, which are the same as those during 1961–2010. Although it is not so consistent, the increasing trend, similar with that in 1961–2010, is also dominant over NE, US, and AU during 1979–2010.

Thus, EAR40 reanalysis data for 1961–2001 (not shown) and studies based on observation data are also employed to verify the reliability of the trends from NCEP-NCAR reanalysis data. We find that the patterns are quite similar between the two reanalysis data. There are widespread increasing trends over EU, US, and AU and decreasing trends over IP and EC, except for the boreal winter half year over EC, in ERA40 reanalysis data, which are similar to those in NCEP-NCAR reanalysis data. These trends are supported by some studies based on radiosonde data. Ross and Elliott (1996, 2001) found that most of the stations over US had an increase trend in precipitable water for all the seasons during 1973–1995. Mattar et al. (2011) also detected decreasing trend for all seasons over IP using radiosonde data for 1973–2003. Radiosonde data showed that most of the stations over EC had a decrease trend in boreal winter during 1979–2005 (Xie et al. 2011). Therefore, the trends in precipitable water from NCEP-NCAR reanalysis data are reliable to a certain extent.

4.2 Trends in static stability during 1961–2010

Precipitation is partly connected with static stability (Peppler and Lamb 1989; Richter and Xie 2008; Johnson and Xie 2010). Temperature difference between lower and upper level

are commonly used to reflect the static stability (Lee and Wang 2014; Liu et al. 2013; Xiang et al. 2014). Actually lapse rate $\gamma = -d7/dz$ involving temperature and altitude differences is more appropriate (Bryan and Fritsch 2000; Joshi et al. 2008). We use the difference of potential height to represent the altitude difference (Stone and Carlson 1979). Figure 6 shows the trends in the atmospheric lapse rate within lower (925–700 hPa) and middle troposphere (850–500 hPa) in boreal summer and winter half year.

It is shown that there are consistent increasing trends in lapse rates within both lower (Fig. 6a) and middle (Fig. 6c) troposphere over EC in boreal summer half year. The regional average lapse rates also exhibit significant increasing trends (Table 3). In boreal winter half year, the lapse rate within lower troposphere is mostly increased over EC, despite an insignificant decreasing trend over south part of EC (Fig. 6b). Furthermore, the lapse rate within middle troposphere has consistent increasing trends over EC (Fig. 6d). The increasing trends in regional average lapse rates within lower and middle troposphere are both evident and significant at the 99 % confidence level (Table 3). The increase in lapse rate is even more evident and consistent over NE. Increasing trends in lapse rates within lower and middle troposphere are widespread across the whole NE in boreal summer and winter half year (Fig. 6). The regional average lapse rates also exhibit significant increasing trends (Table 3). The increase in lapse rates implies that static stability weakens and atmospheric stratification becomes less stable over EC and NE in both boreal summer and winter half year.

In contrast, decreasing trends are found over US, AU, and IP. In boreal summer half year, the lapse rates within lower (Fig. 6a) and middle (Fig. 6c) troposphere decrease across US. The trends in regional average lapse rates are significant at the 95 % confidence level (Table 3). The lapse rates within lower (Fig. 6b) and middle (Fig. 6d) troposphere in boreal winter half year are mainly decreased over US and the regional average lapse rates also have decreasing trends (Table 3). The decline of lapse rates is more evident over AU, where decreasing trends dominate the whole AU in both boreal summer (Fig. 6a, c) and winter (Fig. 6b, d) half year. The trends in regional average lapse rates within lower and middle troposphere are decreased significantly, reaching the 99 % confidence level (Table 3). Over IP, the lapse rate within lower troposphere is decreased consistently in boreal summer half year (Fig. 6a), although the consistence is not so distinct for the lapse rate within middle troposphere (Fig. 6c). What is more, decreasing trends in lapse rates within lower (Fig. 6b) and middle (Fig. 6b) troposphere dominate the entire IP in boreal winter half year. The regional average lapse rates also show decreasing trends in boreal winter half year (Table 3). The decrease in lapse rates indicates that the static stability strengthens and the atmospheric

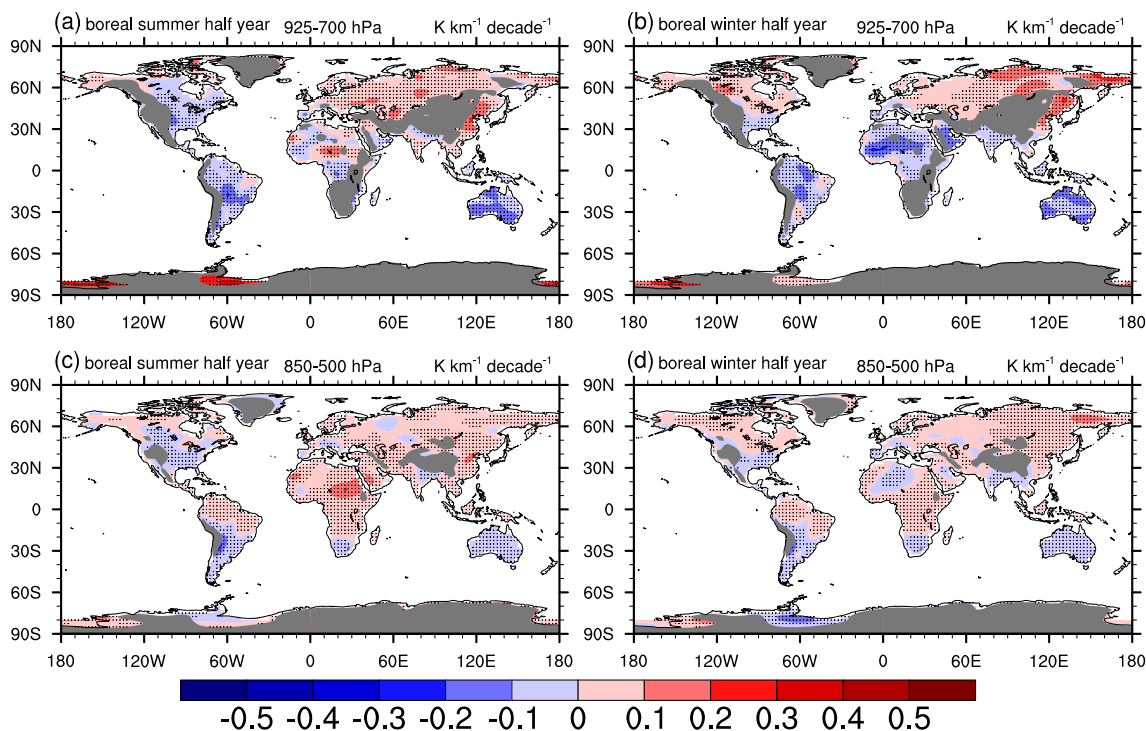


Fig. 6 Trends ($\text{K km}^{-1} \text{ decade}^{-1}$) in atmospheric lapse rate within 925–700 hPa (top row) and 850–500 hPa (bottom row) in boreal summer (left column) and winter (right column) half year based on NCEP-NCAR reanalysis data. Black dots denote the grid points where the trend is

significant at the 90 % confidence level according to Student’s *t* test. Gray color denotes the area where climatology (1981–2010) surface pressure is less than the pressure at the bottom of lapse rate

stratification becomes more stable over US, AU, and IP in boreal summer and winter half year.

4.3 Possible impact of the change of static stability on the trends of light precipitation events

Precipitation is connected with upward motion, and on the other hand, upward motion is associated with atmospheric stratification or static stability. Unstable atmospheric stratification favors upward motion and heavy precipitation; in contrast, stable atmospheric stratification suppresses the upward

motion and precipitation. Hence, when the static stability weakens, the upward motion strengthens and precipitation intensity increases; when the static stability strengthens, the upward motion abates and precipitation intensity decreases.

Associated with the weakening of static stability, the intensity of light precipitation events in boreal summer (Fig. 4c) and winter (Fig. 4d) half year is increased significantly over the EC and NE. What is more, the mean intensity of all the precipitation events is enhanced noticeably in the two regions as well (figure not shown). The increase in intensity leads to a change of the light precipitation events to relatively heavier precipitation events and a decrease in the frequency of light precipitation events correspondingly. In contrast, accompanied with the strengthening of static stability, a decrease in the intensity of light precipitation events is noticeable over US, AU, and IP (Fig. 4c, d). The mean precipitation intensity mainly decreases as well over AU, and IP (figure not shown). The decrease in intensity results in a shift of relatively heavier precipitation events toward light precipitation events and increase in the frequency of light precipitation events consequently.

Furthermore, we employ WRF to examine the impact of static stability on precipitation intensity. The precipitation intensity for the modeling is defined as the daily mean precipitation during the given days (accumulated amount divided by days). The difference of precipitation intensity between

Table 3 Trends ($10^{-3} \text{ K km}^{-1} \text{ decade}^{-1}$) in lapse rate within 925–700 hPa and 850–500 hPa in boreal summer (Sum) and winter (Win) half year over EC, NE, US, AU, and IP, respectively

	925–700 hPa		850–500 hPa	
	Sum	Win	Sum	Win
EC	11.5***	7.4***	5.9***	4.8***
NE	6.6***	8.3***	2.2***	4.7***
US	−4.4***	−1.0	−1.5*	−0.3
AU	−10.1***	−11.4***	−3.3***	−5.5***
IP	−0.9	−4.1**	1.8**	−1.2

*, **, and *** indicate the trends significant at the 90, 95, and 99 % confidence level according to Student’s *t* test

sensitivity experiments and control experiment indicates the effect of static stability on precipitation intensity. The differences of ensemble average precipitation intensity between experiment WEA and experiment CTL for July is dominated by positive value (Fig. 7a), which indicates that precipitation intensity increases as static stability weakens. In contrast, the precipitation differences between experiment STR and experiment CTL are characterized by decreasing change (Fig. 7c), implying that precipitation intensity decreases as static stability strengthens. The regional average precipitation intensity in the three experiments for each day in July (Fig. 8a) reflects that precipitation intensity increases when static stability weakens, and the precipitation intensity decreases when static stability strengthens. The results in January simulation have the same features (Figs. 7b, d; 8b).

The change in precipitation intensity is associated with the change in vertical velocity. The vertical velocities in experiment WEA are larger than those in experiment CTL, but those in experiment STR are smaller (Fig. 8c–f). The differences between control experiment and sensitivity experiment indicate that the vertical velocities increase as static stability weakens and decrease as static stability strengthens. The model results indicate that static stability affects precipitation intensity through upward motion. Precipitation intensity is increased due to the enhancement in upward motion as static stability weakens, and is decreased due to the reduction in upward motion as static stability strengthens.

Hence, the probable mechanism for the impact of static stability on light precipitation events can be summarized as follows: the weakening of static stability leads to increasing of precipitation intensity through the enhancement of upward motion; some light precipitation events become relatively heavier precipitation events and the frequency of light precipitation events decreases correspondingly over EC and NE; in contrast, the strengthening of static stability results in decreasing of precipitation intensity through the reduction of upward motion; some relatively heavier precipitation events turn toward light precipitation events, and the frequency of light precipitation events increase consequently over US, AU, and IP.

5 Conclusions and discussions

In this study, we investigate the trends in light precipitation events over global land and their possible reasons during 1961–2010. Light precipitation event is defined as precipitation event with daily precipitation less than the 50th percentile and above or equal to 0.1 mm/day based on 30-year (1971–2010) daily records. Although reduction is expected according to theoretical speculation and climate models, there is no consistent decreasing trend in the frequency of light precipitation events over global land. There are decreasing trends in annual frequencies of light precipitation events over EC and NE, and

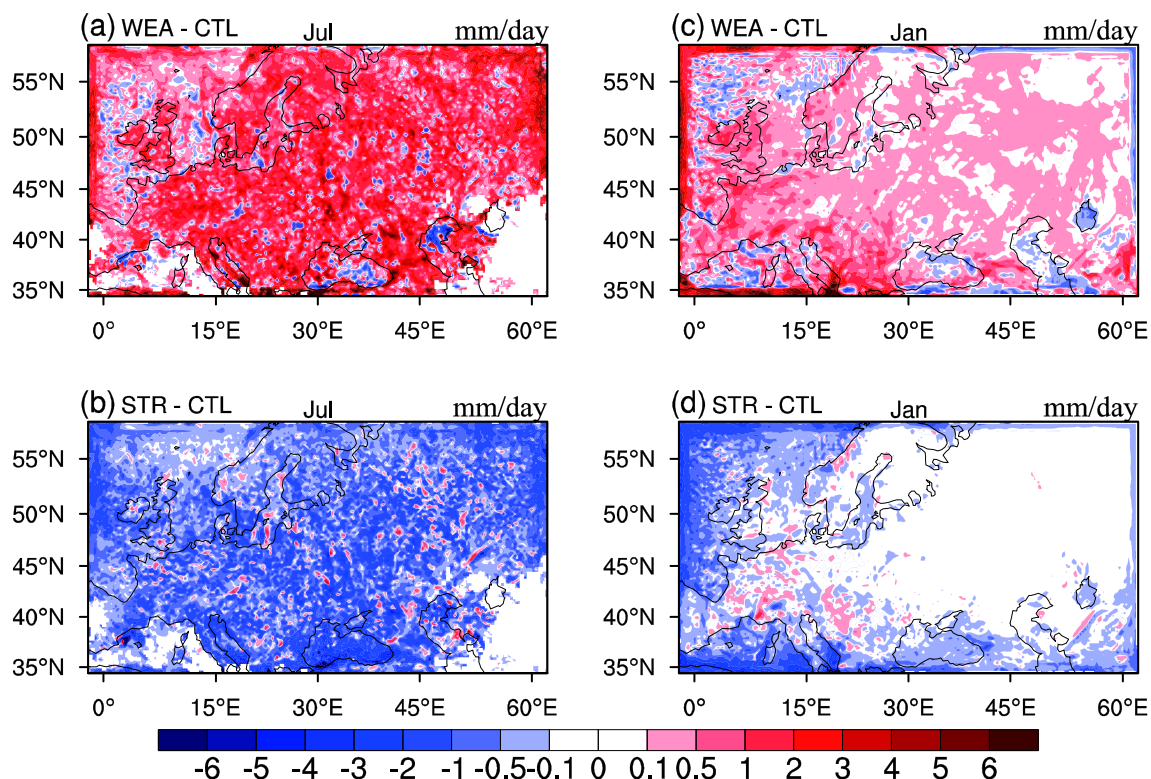
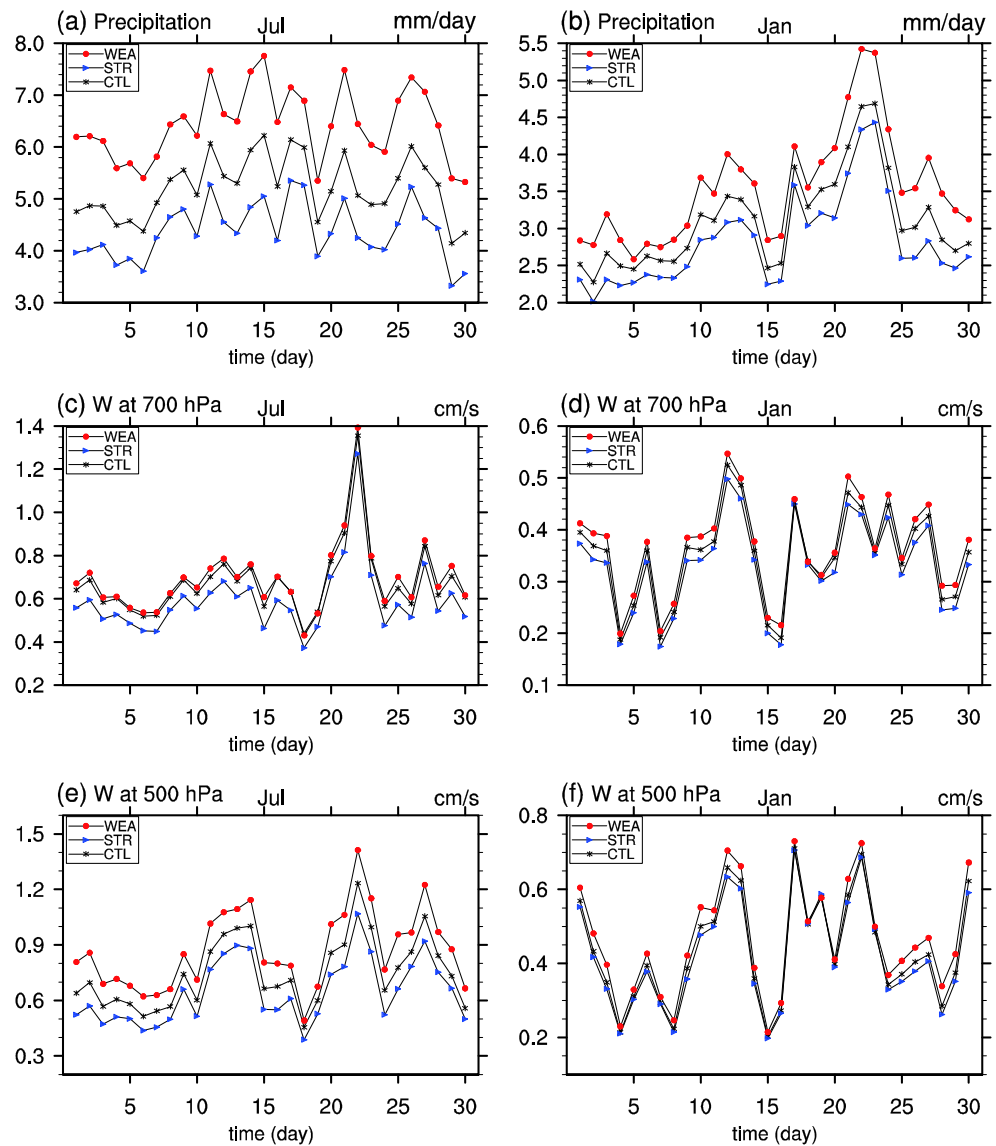


Fig. 7 Precipitation intensity differences (mm/day) between experiment WEA and CTL (*top row*), and between experiment STR and CTL (*bottom row*) in July (Jul, *left column*) and January (Jan, *right column*) simulation

Fig. 8 Regional average (over the areas with daily precipitation above 0.1 mm) precipitation intensity (mm/day, *top row*) and vertical velocity (W , cm/s) at 700 hPa (*second row*) and 500 hPa (*bottom row*) for 30 days in July (*left column*) and January (*right column*). Blue, black, and red lines and markers denote experiment STR, CTL, and WEA, respectively



in contrast, increasing trends over US, AU and the IP. The trends in the intensity of light precipitation events are opposite to those in frequency. The intensity is increased over EC and NE, but is decreased over US, AU, and IP. However, there are no consistent and significant trends in the amounts of light precipitation events except over EC for reverse trends in frequency and intensity. It is interesting to note that the trends in light precipitation events for boreal summer and winter half year are similar to the trends for annual events. The frequency is decreased and the intensity is increased over EC and NE in boreal summer and winter half year, but the frequency is increased and the intensity is decreased over US, AU, and IP.

Although we reveal the trends in light precipitation over a large part of global land, there are still some regions including Africa and South America where the trends are unknown due to data deficiency. The lack of data makes it unable to detect climate change of extreme precipitation events over Africa

and South America (Alexander et al. 2006; Giorgi et al. 2011; Donat et al. 2013).

Additionally, we investigate the possible reasons for the trends in light precipitation events. We have examined the change of atmospheric water vapor. However, we have not found creditable linkage between atmospheric water vapor and light precipitation. Further analysis suggests that the trends in light precipitation events are possibly due to the changes in static stability. The static stability weakens and the atmospheric stratification becomes less stable over EC and NE, but the static stability strengthens and the atmospheric stratification becomes more stable over US, AU, and IP. The weakening of static stability leads to increasing of precipitation intensity through the enhancement of upward motion; light precipitation events turn to relatively heavier precipitation events and the frequency decreases correspondingly over EC and NE; in contrast, the strengthening of static stability

results in decreasing of precipitation intensity due to the reduction of upward motion; relatively heavier precipitation events shift toward light precipitation events and the frequency of light precipitation events increases consequently over US, AU, and IP.

However, the cause of the change of static stability is still unknown. It is largely associated with the change of troposphere temperature, which is possibly connected with the change of atmospheric radiation and atmospheric circulation. We will investigate this issue in the near future.

Acknowledgments This work was supported by the National Basic Research Program of China (2012CB955604 and 2011CB309704), the National Science Fund for Distinguished Young Scholars (41425019), the National Natural Science Foundation of China (41275083 and 91337105), the Scientific Research Starting Foundation of Guangzhou Institute of Tropical and Marine Meteorology (1420200137), and the Guangdong Science and Technology Plan Project (2012A061400012).

References

- Alexander LV et al (2006) Global observed changes in daily climate extremes of temperature and precipitation. *J Geophys Res* 111: D05109. doi:10.1029/2005jd006290
- Allan RP, Soden BJ (2008) Atmospheric warming and the amplification of precipitation extremes. *Science* 321:1481–1484. doi:10.1126/science.1160787
- Allen MR, Ingram WJ (2002) Constraints on future changes in climate and the hydrologic cycle. *Nature* 419:224–232. doi:10.1038/nature01092
- Boer GJ (1993) Climate change and the regulation of the surface moisture and energy budgets. *Clim Dyn* 8:225–239. doi:10.1007/bf00198617
- Bryan GH, Fritsch JM (2000) Moist absolute instability: the sixth static stability state. *Bull Am Meteorol Soc* 81:1207–1230. doi:10.1175/1520-0477(2000)081<1287:MAITSS>2.3.CO;2
- Caesar J, Alexander L, Vose R (2006) Large-scale changes in observed daily maximum and minimum temperatures: creation and analysis of a new gridded data set. *J Geophys Res Atmos* 111:D05101. doi:10.1029/2005jd006280
- Donat MG et al (2013) Updated analyses of temperature and precipitation extreme indices since the beginning of the twentieth century: the HadEX2 dataset. *J Geophys Res Atmos* 118:2098–2118. doi:10.1002/jgrd.50150
- Durre I, Menne MJ, Gleason BE, Houston TG, Vose RS (2010) Comprehensive automated quality assurance of daily surface observations. *J Appl Meteorol Climatol* 49:1615–1633. doi:10.1175/2010jamec2375.1
- Easterling DR, Evans JL, Groisman PY, Karl TR, Kunkel KE, Ambenje P (2000) Observed variability and trends in extreme climate events: a brief review. *Bull Am Meteorol Soc* 81:417–425. doi:10.1175/1520-0477(2000)081<0417:ovatie>2.3.co;2
- Fujibe F, Yamazaki N, Katsuyama M, Kobayashi K (2005) The increasing trend of intense precipitation in Japan based on four-hourly data for a hundred years. *SOLA* 1:41–44. doi:10.2151/sola.2005-012
- Giorgi F, Im ES, Coppola E, Diffenbaugh NS, Gao XJ, Mariotti L, Shi Y (2011) Higher hydroclimatic intensity with global warming. *J Clim* 24:5309–5324. doi:10.1175/2011jcli3979.1
- Goswami BN, Venugopal V, Sengupta D, Madhusoodanan MS, Xavier PK (2006) Increasing trend of extreme rain events over India in a warming environment. *Science* 314:1442–1445. doi:10.1126/science.1132027
- Groisman PY et al (1999) Changes in the probability of heavy precipitation: important indicators of climatic change. *Clim Chang* 42:243–283. doi:10.1023/a:1005432803188
- Groisman PY, Knight RW, Easterling DR, Karl TR, Hegerl GC, Razuvaev VN (2005) Trends in intense precipitation in the climate record. *J Clim* 18:1326–1350. doi:10.1175/jcli3339.1
- Held IM, Soden BJ (2006) Robust responses of the hydrological cycle to global warming. *J Clim* 19:5686–5699. doi:10.1175/jcli3990.1
- Hennessy KJ, Gregory JM, Mitchell JFB (1997) Changes in daily precipitation under enhanced greenhouse conditions. *Clim Dyn* 13: 667–680. doi:10.1007/s003820050189
- Huang G, Wen G (2013) Spatial and temporal variations of light rain events over China and the mid-high latitudes of the Northern Hemisphere. *Chin Sci Bull* 58:1402–1411. doi:10.1007/s11434-012-5593-1
- Johnson NC, Xie S-P (2010) Changes in the sea surface temperature threshold for tropical convection. *Nat Geosci* 3:842–845. doi:10.1038/ngeo1008
- Joshi M, Gregory J, Webb M, Sexton DH, Johns T (2008) Mechanisms for the land/sea warming contrast exhibited by simulations of climate change. *Clim Dyn* 30:455–465. doi:10.1007/s00382-007-0306-1
- Kalnay E et al (1996) The NCEP/NCAR 40-year reanalysis project. *Bull Am Meteorol Soc* 77:437–471. doi:10.1175/1520-0477(1996)077<0437:tnyrp>2.0.co;2
- Karl TR, Knight RW (1998) Secular trends of precipitation amount, frequency, and intensity in the United States. *Bull Am Meteorol Soc* 79:231–241. doi:10.1175/1520-0477(1998)079<0231:stopaf>2.0.co;2
- Karl TR, Trenberth KE (2003) Modern global climate change. *Science* 302:1719–1723. doi:10.1126/science.1090228
- Kiktev D, Sexton DMH, Alexander L, Folland CK (2003) Comparison of modeled and observed trends in indices of daily climate extremes. *J Clim* 16:3560–3571. doi:10.1175/1520-0442(2003)016<3560:comaot>2.0.co;2
- Kistler R et al (2001) The NCEP–NCAR 50-year reanalysis: monthly means CD-ROM and documentation. *Bull Am Meteorol Soc* 82: 247–267. doi:10.1175/1520-0477(2001)082<0247:tnnyrm>2.3.co;2
- Klein Tank AMG, Können GP (2003) Trends in indices of daily temperature and precipitation extremes in Europe, 1946–99. *J Clim* 16: 3665–3680. doi:10.1175/1520-0442(2003)016<3665:tiiodt>2.0.co;2
- Klein Tank AMG et al (2002) Daily dataset of 20th-century surface air temperature and precipitation series for the European Climate Assessment. *Int J Climatol* 22:1441–1453. doi:10.1002/joc.773
- Kunkel KE, Andsager K, Easterling DR (1999) Long-term trends in extreme precipitation events over the conterminous United States and Canada. *J Clim* 12:2515–2527. doi:10.1175/1520-0442(1999)012<2515:lttiep>2.0.co;2
- Lee J-Y, Wang B (2014) Future change of global monsoon in the CMIP5. *Clim Dyn* 42:101–119. doi:10.1007/s00382-012-1564-0
- Liu SC, Fu C, Shiu C-J, Chen J-P, Wu F (2009) Temperature dependence of global precipitation extremes. *Geophys Res Lett* 36:L17702. doi:10.1029/2009gl040218
- Liu J, Wang B, Cane MA, Yim S-Y, Lee J-Y (2013) Divergent global precipitation changes induced by natural versus anthropogenic forcing. *Nature* 493:656–659. doi:10.1038/nature11784
- Mattar C, Sobrino JA, Julien Y, Morales L (2011) Trends in column integrated water vapour over Europe from 1973 to 2003. *Int J Climatol* 31:1749–1757. doi:10.1002/joc.2186
- Menne MJ, Durre I, Vose RS, Gleason BE, Houston TG (2012) An overview of the global historical climatology network-daily database. *J Atmos Ocean Technol* 29:897–910. doi:10.1175/jtech-d-11-00103.1

- National Centers for Environmental Prediction NWS, NOAA, U. S. Department of Commerce (2000) NCEP FNL Operational model global tropospheric analyses, continuing from July 1999. Research Data Archive at the National Center for Atmospheric Research, Computational and Information Systems Laboratory, Boulder
- New M, Hulme M, Jones P (2000) Representing twentieth-century space–time climate variability. Part II: development of 1901–96 monthly grids of terrestrial surface climate. *J Clim* 13:2217–2238. doi:10.1175/1520-0442(2000)013<2217:rtcstc>2.0.co;2
- Osborn TJ, Hulme M, Jones PD, Basnett TA (2000) Observed trends in the daily intensity of United Kingdom precipitation. *Int J Climatol* 20:347–364. doi:10.1002/(sici)1097-0088(20000330)20:4<347::aid-joc475>3.0.co;2-c
- Pall P, Allen M, Stone D (2007) Testing the Clausius–Clapeyron constraint on changes in extreme precipitation under CO₂ warming. *Clim Dyn* 28:351–363. doi:10.1007/s00382-006-0180-2
- Peppler RA, Lamb PJ (1989) Tropospheric static stability and Central North American growing season rainfall. *Mon Weather Rev* 117:1156–1180. doi:10.1175/1520-0493(1989)117<1156:tssacn>2.0.co;2
- Qian Y, Gong DY, Fan JW, Leung LR, Bennartz R, Chen D, Wang WG (2009) Heavy pollution suppresses light rain in China: observations and modeling. *J Geophys Res Atmos* 114:D00K02. doi:10.1029/2008jd011575
- Qian Y, Gong DY, Leung R (2010) Light rain events change over North America, Europe, and Asia for 1973–2009. *Atmos Sci Lett* 11:301–306. doi:10.1002/Asl.298
- Richter I, Xie S-P (2008) Muted precipitation increase in global warming simulations: a surface evaporation perspective. *J Geophys Res Atmos* 113:D24118. doi:10.1029/2008jd010561
- Ross RJ, Elliott WP (1996) Tropospheric water vapor climatology and trends over North America: 1973–93. *J Clim* 9:3561–3574. doi:10.1175/1520-0442(1996)009<3561:twvcat>2.0.co;2
- Ross RJ, Elliott WP (2001) Radiosonde-based northern hemisphere tropospheric water vapor trends. *J Clim* 14:1602–1612. doi:10.1175/1520-0442(2001)014<1602:rbnhtw>2.0.co;2
- Shepard D (1968) A two-dimensional interpolation function for irregularly-spaced data. Paper presented at the Proceedings of the 1968 23rd ACM national conference
- Shepard D (1984) Computer mapping: the SYMAP interpolation algorithm. In: Gaile G, Willmott C (eds) *Spatial statistics and models*, vol 40. Theory and decision library, vol 40. Springer, Netherlands, pp 133–145. doi:10.1007/978-94-017-3048-8_7
- Shiu C-J, Liu SC, Fu C, Dai A, Sun Y (2012) How much do precipitation extremes change in a warming climate? *Geophys Res Lett* 39:L17707. doi:10.1029/2012gl052762
- Stone PH, Carlson JH (1979) Atmospheric lapse rate regimes and their parameterization. *J Atmos Sci* 36:415–423. doi:10.1175/1520-0469(1979)036<0415:alrrat>2.0.co;2
- Sun Y, Solomon S, Dai A, Portmann RW (2007) How often will it rain? *J Clim* 20:4801–4818. doi:10.1175/jcli4263.1
- Suppiah R, Hennessy KJ (1998) Trends in total rainfall, heavy rain events and number of dry days in Australia, 1910–1990. *Int J Climatol* 18:1141–1164. doi:10.1002/(sici)1097-0088(199808)18:10<1141::aid-joc286>3.0.co;2-p
- Trenberth KE (1998) Atmospheric moisture residence times and cycling: implications for rainfall rates and climate change. *Clim Chang* 39:667–694. doi:10.1023/A:1005319109110
- Trenberth KE (1999) Conceptual framework for changes of extremes of the hydrological cycle with climate change. *Clim Chang* 42:327–339. doi:10.1023/A:1005488920935
- Trenberth KE (2011) Changes in precipitation with climate change. *Clim Res* 47:123–138. doi:10.3354/cr00953
- Trenberth KE, Dai A, Rasmussen RM, Parsons DB (2003) The changing character of precipitation. *Bull Am Meteorol Soc* 84:1205–1217. doi:10.1175/bams-84-9-1205
- Trenberth KE et al (2007) Observations: surface and atmospheric climate change. In: Solomon S, Qin D, Manning M, Marquis M, Averyt K, Tignor MMB, Miller HL (eds) *Climate Change 2007: the physical science basis. Contribution of working group I to the fourth assessment report of the intergovernmental panel on climate change*. Cambridge University Press, Cambridge, pp 235–336
- Wen G, Huang G, Hu K, Qu X, Tao W, Gong H (2015) Changes in the characteristics of precipitation over northern Eurasia. *Theor Appl Climatol* 119:653–665. doi:10.1007/s00704-014-1137-8
- Xiang B, Wang B, Lauer A, Lee J-Y, Ding Q (2014) Upper tropospheric warming intensifies sea surface warming. *Clim Dyn* 43:259–270. doi:10.1007/s00382-013-1928-0
- Xie B, Zhang Q, Ying Y (2011) Trends in precipitable water and relative humidity in China: 1979–2005. *J Appl Meteorol Climatol* 50:1985–1994. doi:10.1175/2011jamc2446.1
- Zhai PM, Zhang XB, Wan H, Pan XH (2005) Trends in total precipitation and frequency of daily precipitation extremes over China. *J Clim* 18:1096–1108. doi:10.1175/JCLI-3318.1
- Zhang X, Hogg WD, Mekis É (2001) Spatial and temporal characteristics of heavy precipitation events over Canada. *J Clim* 14:1923–1936. doi:10.1175/1520-0442(2001)014<1923:satcoh>2.0.co;2
- Zveryaev II, Chu P-S (2003) Recent climate changes in precipitable water in the global tropics as revealed in National Centers for Environmental Prediction/National Center for Atmospheric Research reanalysis. *J Geophys Res Atmos* 108:4311. doi:10.1029/2002jd002476